COMPARISON OF SART AND ETV RECONSTRUCTION FOR INCREASED C-ARM CT VOLUME COVERAGE BY PROPER DETECTOR ROTATION IN LIVER IMAGING

D. Stromer[1], *M. Amrehn*[1,2], *Y. Huang*[1,2], *P. Kugler*[2], *S. Bauer*[2], *G. Lauritsch*[2] *and A. Maier*[1,3]

[1]Pattern Recognition Lab, FAU Erlangen-Nuremberg
[2]Siemens Healthcare GmbH, Forchheim, Germany
[3]Erlangen Graduate School in Advanced Optical Technologies (SAOT)

ABSTRACT

In this work, we present a method to increase the lateral field-of-view of a C-arm CT system by rotating the detector such that the diagonal of the detector lies on the u-axis of the detector's coordinate system. We investigated three different 3-D scan trajectories for liver imaging of an obese patient (waist circumference 130 cm) – a Short Scan, a Large Volume Scan and a Helical Large Volume Scan. We reconstructed a data set of the Visible Human Project with the SART and the eTV algorithm. Tests revealed that the coverage was increased with the presented method by 25.3 % for the Short Scan and 28.5 % for the Large Volume Scan. Performing helical scans compensated the axial data loss. The two implemented iterative approaches both provide acceptable results, with the eTV algorithm reducing the RMSE compared to SART by about 29 %. Given a liver imaging task, the rotated detector is able to image the entire liver section of the abdomen with a single Large Volume Scan.

Index Terms— eTV, iTV, SART, Diamond Scan, Field-of-View Enlargement, Iterative Reconstruction

Disclaimer: The concepts and information presented in this paper are based on research and are not commercially available.

1. INTRODUCTION

Current Robotic C-arm X-ray systems allow to calibrate a wide range of trajectories [1]. The two most common 3-D scan modes with those systems use circular scan trajectories. The Short Scan [2] performs a turn of $180\,^\circ$ plus fan angle while the Large Volume Scan (LVS) [3] performs a $360\,^\circ$ rotation with a detector shift of a half detector width in lateral detector direction nearly doubling the field-of-view. Situations occur in the clinical workflow where the volume-of-interest is still too large to cover it properly with those scans, for example if the liver of a large patient or the whole abdomen have to be shown. Therefore, a method is presented, where the detector is rotated properly to extend the field-of-view. However, this comes at an axial loss perpendicular to the central slice. A helical trajectory with a small pitch can be applied for the LVS with the aim to compensate this loss.

To reconstruct the volumes, we selected two iterative reconstruction approaches. The Simultaneous Algebraic Reconstruction Technique (SART) reconstructs a volume by volume forward projections and corrective back projections. The Enhanced Total Variation Constraint Reconstruction (eTV) is a total variation based method with the aim to keep the raw data fidelity high and getting a piecewise constant output [4]. It extends the SART algorithm by an additional constraint based on the theory of Compressed Sensing.

2. MATERIALS AND METHODS

For all tests, the CONRAD [5] framework for cone beam imaging in radiology was used. The test system consists of a $400\,\mathrm{mm} \times 300\,\mathrm{mm}$ detector with a spacing of $1\,\mathrm{mm} \times 1\,\mathrm{mm}$. The source-to-object distance (SOD) was set to $785\,\mathrm{mm}$ and the source-to-intensifier distance (SID) to $1200\,\mathrm{mm}$. The theoretically obtainable coverage c is calculated by $c = SOD \cdot SID^{-1} \cdot u_{spread}$ with u_{spread} denoting the current lateral field-of-view spread.

2.1. Diamond Scan

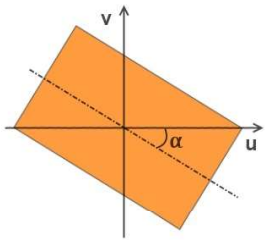

Fig. 1. Detector rotated by angle α.

The enlargement of the field-of-view is achieved by rotating the system's detector such that the diagonal lies on the u-axis. The rotation angle α results from $v_{max} \cdot u_{max}^{-1}$ where u_{max} is the maximal width and v_{max} the maximal height of

the detector. For the given measurements, the lateral spread is increased by $25\,\%$ from $400\,\mathrm{mm}$ to $500\,\mathrm{mm}$. However, the shape of the coverage will be diamond shaped with a maximal lateral spread along the u-axis of the detector.

2.2. Scan modes

The first investigated scan mode is a Short Scan performing a circular rotation of $200\,^\circ$ ($180\,^\circ$ plus fan angle) for getting a minimal complete dataset. For the tests, 266 projections resulting in an average angular increment of $0.75\,^\circ$ were selected. The standard coverage diameter is $261.7\,\mathrm{mm}$. Applying the Diamond Scan should increase this by about $65\,\mathrm{mm}$ to $327\,\mathrm{mm}$.

The second scan is the Large Volume Scan (LVS) which performs a $360\,^\circ$ rotation with a detector shift of half the detector width being able to double up the coverage. The coverage for this scan reaches $523\,\mathrm{mm}$ and with the Diamond Scan it can be increased up to $654\,\mathrm{mm}$. In practice, an overlap of $20\,\%$ is configured to ensure data completeness around the rotation center. This adaption results in an achievable standard LVS coverage of $471\,\mathrm{mm}$. With an overlap of $15\,\%$ the Diamond LVS extends the coverage to $605\,\mathrm{mm}$.

However, applying the detector rotation results in an axial coverage loss which could potentially pose problems for the liver imaging task. To alleviate the problem, a Helical LVS trajectory with a small pitch of $20\,\mathrm{mm}$ and three rotations is investigated. Note that such a scan path cannot be implemented on a real angiography system since they typically allow at most $400\,^\circ$ of rotation.

2.3. 3-D Reconstruction

In this work, two different iterative reconstruction methods were implemented fully GPU-based and tested with all scan modes. Those approaches solve the inverse Radon transform problem by minimizing an objective function which can also incorporate prior knowledge. The implemented methods use a SSD measure as objective function minimizing the difference between the projection raw data p and the projected current image, resulting from the Radon transform R of the reconstructed image $f(\boldsymbol{r})$ with the specific voxel $\boldsymbol{r} = (r_1, r_2, r_3)$:

$$min||R\,f(\boldsymbol{r}) - p||_2^2 \tag{1}$$

2.3.1. Simultaneous Algebraic Reconstruction Technique

SART performs forward projections and corrective back projections until the reconstructed volume data have converged. The voxel volume is updated simultaneously after all projection rays are processed [6]. An initial volume is estimated and the orthogonal projections to the hyperplanes are calculated by back projection. Their centroid is saved and used for the next iteration. The update rule is given by

$$f_i^{\nu+1} = f_i^{\nu} + \beta \sum_{k \in s(\nu)} \frac{1}{\sum_j (\boldsymbol{R}^\top)_{i,j}^k} (\boldsymbol{R}^\top)_{i,j}^k \frac{\sum_i \boldsymbol{R}_{j,i}^k f_i^{\nu} - p_j^k}{\sum_i \boldsymbol{R}_{j,i}^k} \tag{2}$$

with $\nu \in [0, N_{Sub}[$. i denotes the index of volume voxel $\boldsymbol{r}$ whereas j is the index of one projection element. k denotes the index of a subset's projection such that $\boldsymbol{R}_{j,i}^k$ is the Radon transform of projection k mapping f on p^k. N_{Proj} denotes the number of projections while N_{Sub} is the number of subsets and ν the index of the subset. $s(\nu)$ represents the number of projections inside a subset while β is the relaxation parameter used to control the convergence speed of the minimization. In this work, N_{Sub} was set to N_{Proj} leading to a subset size $s(\nu)$ of 1. This means, that every projection is handled separately. f_{n+1}^{SART} denotes a complete SART iteration where n equals the number of completed iterations of the update step.

2.3.2. Enhanced Total Variation Constraint Reconstruction

eTV is a method incorporating an a priori knowledge constraint into the Iterative Reconstruction [4] based on the Improved Total Variation Constraint Reconstruction (iTV) [7]. The constraint is based on the theory of Compressed Sensing stating that $f(\boldsymbol{r})$ can be reconstructed with a high probability with less samples than required by the Nyquist-Shannon theorem if most entries of its sparsifying transformation $\Psi(\boldsymbol{r})$ are zero. This can be approximated by the $l1$-norm leading to the convex optimization function

$$min||\Psi f(\boldsymbol{r})||_1 \text{ subject to } ||\boldsymbol{R}\,f(\boldsymbol{r}) - p||_2^2 < \epsilon \tag{3}$$

minimizing the raw data cost function incorporating the sparsity constraint. iTV minimizes the raw data cost function via SART. The sparsity is handled separately with the image gradient as sparsifying transformation Ψ and a Gradient Descent approach, consisting of M steps in each outer iteration to reduce the Total Variation cost function $||\nabla f(\boldsymbol{r})||_1$:

$$f_{n+1,m+1}^{TV}(\boldsymbol{r}) = f_{n+1,m}^{TV}(\boldsymbol{r}) - \alpha \cdot \nabla||\nabla f_{n+1,m}^{TV}(\boldsymbol{r})||_1 \tag{4}$$

where $\nabla||\nabla f_{n+1,m}^{TV}||_1$ is approximated by

$$\frac{\nabla_{xx} f_{n+1,m}^{TV} + \nabla_{yy} f_{n+1,m}^{TV} + \nabla_{zz} f_{n+1,m}^{TV}}{\sqrt{(\nabla_x f_{n+1,m}^{TV})^2 + (\nabla_y f_{n+1,m}^{TV})^2 + (\nabla_z f_{n+1,m}^{TV})^2 + reg^2}}. \tag{5}$$

A complete iTV iteration is formed by the linear combination of the two subsequent images by

$$f_{n+1} = (1-\lambda) f_{n+1}^{SART}(\boldsymbol{r}) + \lambda f_{n+1,M}^{TV}(\boldsymbol{r}) \tag{6}$$

with a weighting factor $\lambda \in]0;1]$ where λ is derived by minimizing

$$\epsilon_{n+1} = ||R[(1-\lambda) f_{n+1}^{SART}(\boldsymbol{r}) + \lambda f_{n+1,M}^{TV}(\boldsymbol{r})] - p||_2^2 \tag{7}$$

meanwhile

$$(1-\omega)\cdot||Rf_{n+1}^{SART}(\boldsymbol{r})-p||_2^2+\omega\epsilon_n=\epsilon_{n+1} \quad (8)$$

is calculated previously with the user parameter $\omega \in [0;1]$. High values of ω decrease the convergence speed of the reconstruction, giving more weight to the TV minimization in the process. As those calculations do not allow to perform more than one TV minimization iteration or a value $\lambda > 1$, eTV improves this method by defining a value $\lambda_{max} > 1$ enabling to repeat the TV minimization and the linear combination until $\lambda < \lambda_{max}$. For the simulations, λ_{max} was set to 1.2 and 10 eTV iterations were configured.

3. RESULTS

Method	β	w	reg	M	α_{init}	Iterations
SART	0.3	n.a.	n.a.	n.a.	n.a.	50
eTV	0.2	0.8	10^{-4}	25	0.3	100

Table 1. Reconstruction settings

Tab. 1 shows the selected settings for all reconstructions. The volume is a $320 \times 320 \times 30$ voxel volume with a spacing of 1 mm taken from the Visible Human Project's normal CT male dataset in the abdominal area. The volume was scaled to have a waist circumference of 130 cm which is less or equal to 5 % of the US American population's measures [8]. Because the patients are usually not that large, a transversal misalignment of 10 % (32 mm) was assumed. As error measurement, the RMSE was chosen. Tab. 2 shows the results of the implemented algorithms for all investigated scan modes. eTV reduces the RMSE of SART by 29.1 %, however, this comes with an increased computation time by a factor of 4.8.

Scan Mode	$RMSE_{SART}$	$RMSE_{eTV}$
Short	0.2134	0.1370
Diamond Short	0.2026	0.1242
LVS	0.0608	0.0549
Diamond LVS	0.0322	0.0217
Helix LVS	0.0641	0.0488
Helix Diamond	0.0229	0.0151
Average eTV Improvement:		29.1 %

Table 2. Reconstruction results of the real patient data showing an RMSE improvement of 29.1 %.

Fig. 2 shows the central slices of the eTV reconstructions, where one can see the increased coverage of the Diamond Scans. With the misaligned object, the standard LVS is not able to cover the whole abdominal area properly, while the Diamond LVS can. The measured coverages match exactly with the theoretically achievable coverages. Fig. 3 shows that in the outmost slice ($z = 30$), the Diamond LVS does not cover the complete volume around the origin but the helical scan compensates this axial data loss. When looking at the xz-layer of the scans (Fig. 4), one can see the obtained diamond-shaped coverage for Diamond Short Scan. Also the axial compensation by the Helical Diamond LVS around the origin can be seen. Fig. 5 shows the achieved coverage extension for all scans in total matching exactly with the theoretically achievable coverages. The coverage for the Short Scan is increased by 25.3 %, the LVS's coverage by 28.5 %.

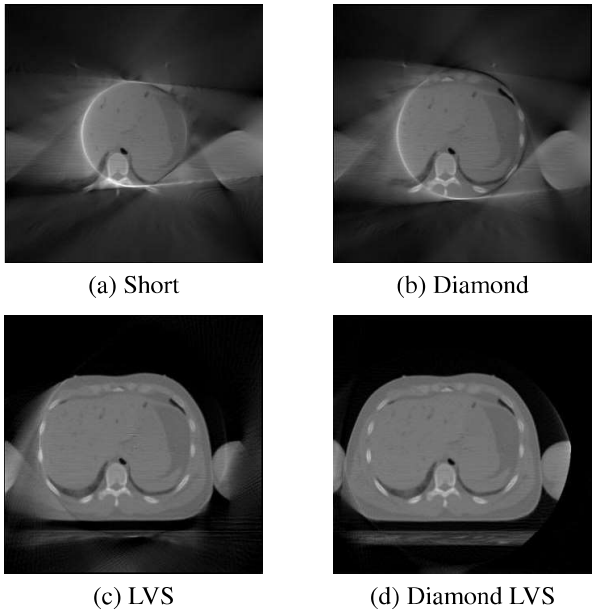

(a) Short (b) Diamond

(c) LVS (d) Diamond LVS

Fig. 2. Central slices of the eTV reconstructions.

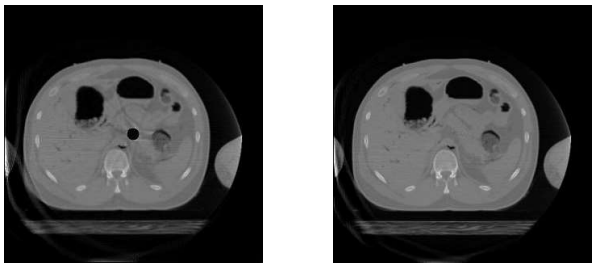

(a) Diamond LVS (b) Helix Diamond LVS

Fig. 3. Outmost slices of the eTV reconstructions for the Circular and the Helix Diamonds LVSs showing the axial coverage compensation around the origin.

4. DISCUSSION AND CONCLUSION

In this work, we presented a method to enlarge the lateral field-of-view of a C-arm CT system by applying a detector

rotation such that the diagonal of the detector lies on the u-axis of its coordinate system. We achieved a coverage diameter plus of $66\,\mathrm{mm}$ for the Short Scan and $134\,\mathrm{mm}$ for the LVS. Axial loss around the center for the LVSs are compensated by utilizing helical instead of circular trajectories. One could also think about trade-off configurations for the detector shift, which also compensates the axial loss while still gaining increased lateral coverage. The eTV algorithm reduced the RMSE compared to SART by about $29\,\%$, however, both algorithms provide acceptable results. Performing a parameter optimization for the eTV method could reduce the errors even more, but the images may get too smooth if one does not pay attention to the regularization. In practice, the LVS is able to cover the whole abdomen for patients with a waist circumference up to $130\,\mathrm{cm}$. The presented method enables the acquisition of patients with a waist circumference up to $180\,\mathrm{cm}$, enabling acquiring medical images for the treatment of an additional $5\,\%$ of the US American population. The volume will even be covered when misalignments in transversal direction occur. For the liver application, the additional data gathered using a helix trajectory did not yield a lot of additional improvement. Thus, the method can be implemented on a real angiographic C-arm system.

(a) Short

(b) Diamond

(c) LVS

(d) Diamond LVS

(e) Helix Diamond LVS

Fig. 4. xz-layer of the volume's eTV reconstructions.

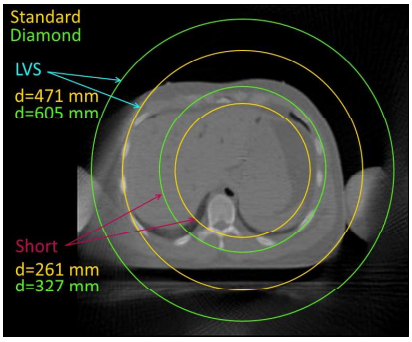

Fig. 5. Comparison of the scan modes lateral coverages. The yellow color denotes the standard Scans, the green color the Diamond Scans while d denotes the circles' diameter in mm.

5. REFERENCES

[1] Magdalena Herbst, Frank Schebesch, Martin Berger, Jang-Hwan Choi, Rebecca Fahrig, Joachim Hornegger, and Andreas Maier, "Dynamic detector offsets for field of view extension in c-arm computed tomography with application to weight-bearing imaging," *Medical Physics*, pp. 2718–2729, 2015.

[2] Dennis L Parker, "Optimal short scan convolution reconstruction for fan beam ct," *Medical physics*, vol. 9, no. 2, pp. 254–257, 1982.

[3] Norbert Strobel, Oliver Meissner, Jan Boese, Thomas Brunner, Benno Heigl, Martin Hoheisel, Ernst-Peter Rührnschopf, Günter Lauritsch, Markus Nagel, Marcus Pfister, et al., "3d imaging with flat-detector c-arm systems," in *Multislice CT*, pp. 33–51. Springer, 2009.

[4] Mario Amrehn, *Implementation and Evaluation of a Total Variation Regularized Iterative CT image Reconstruction Method*, Friedrich-Alexander-University Erlangen-Nuremberg, 2014.

[5] Andreas Maier, Hannes G Hofmann, Martin Berger, Peter Fischer, Chris Schwemmer, Haibo Wu, Kerstin Müller, Joachim Hornegger, Jang-Hwan Choi, Christian Riess, Andreas Keil, and Rebecca Fahrig, "Conrad - a software framework for cone-beam imaging in radiology," *Medical Physics*, vol. 40, no. 11, 2013.

[6] Klaus Mueller, *Fast and accurate three-dimensional reconstruction from cone-beam projection data using algebraic methods*, Ph.D. thesis, The Ohio State University, 1998.

[7] Ludwig Ritschl, Frank Bergner, Christof Fleischmann, and Marc Kachelrieß, "Improved total variation-based ct image reconstruction applied to clinical data," *Physics in medicine and biology*, vol. 56, no. 6, pp. 1545, 2011.

[8] Cheryl D Fryar, Qiuping Gu, and Cynthia L Ogden, "Anthropometric reference data for children and adults: United states, 2007-2010.," *Vital and health statistics. Series 11, Data from the national health survey*, , no. 252, pp. 1–48, 2012.